JOC The Journal of Organic Chemistry

Article

pubs.acs.org/joc

Switching Off the Charge Transfer and Closing the S_1-T_1 ISC Channel in Excited States of Quinolizinium Derivatives: A Theoretical Study

Soydan Yalcin,[†] Laura Thomas,[‡] Maoqun Tian,[‡] Nurgul Seferoglu,[§] Heiko Ihmels,*[,‡] and Yavuz Dede*[,†]

[†]Department of Chemistry, Faculty of Science, Gazi University, Teknikokullar, Ankara 06500, Turkey

[‡]Organische Chemie II, Universität Siegen, Adolf-Reichwein-Straße 2, 57068 Siegen, Germany

[§]Graduate School of Natural and Applied Sciences, Advanced Technologies, Gazi University, Ankara 06500, Turkey

Supporting Information

ABSTRACT: Excited states of benzo[*b*]quinolizinium (**BQ**) derivatives that show efficient pH-responsive fluorescence switching properties were studied quantum-chemically by employing the CASSCF/CASPT2 and TD-DFT methods. Protonation of amino-phenyl-**BQ** at the electron-donor amine moiety converts the nitrogen lone pair into a σ bond and the HOMO into a lower-lying orbital that is no longer involved in the excitation, thereby rationalizing the suppression of the charge transfer. An S_1-T_1 seam between the vertically excited Franck–Condon (FC) point and the S_1 equilibrium geometry favors intersystem crossing (ISC). The T_1 state of the protonated form remains well below S_1 (1.5 eV) because of favorable exchange interactions, whereas the T_1 state of the unprotonated form does not experience any analogous stabilization because of the difference in the spatial domains of the singly occupied orbitals in the S_1 and T_1 states. The S_1 surface from the FC point until the equilibrium geometry for the protonated species is energetically downhill. Calculations on models and available experimental data suggest design principles for similarly functioning pH-responsive species, namely, an amine lone pair as the electron donor and a cationic ring of moderate size as the electron acceptor that are structurally separated by virtue of a spacer.

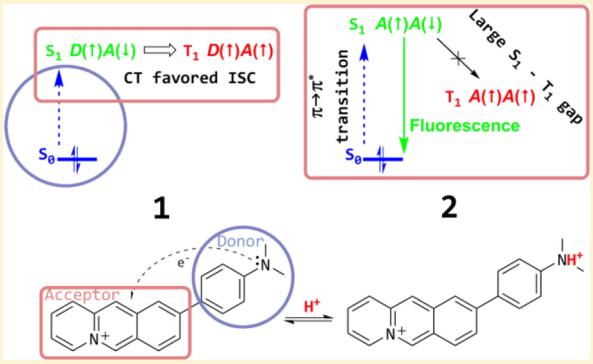

INTRODUCTION

Organic fluorescent probes are attractive and versatile tools in sensor applications, as they enable highly sensitive and selective detection of biologically and/or environmentally relevant analytes at low concentrations. A vast library of readily available compounds is routinely utilized for optical detection of various analytes by quantitative studies of emission energy, emission quantum yield, or emission lifetime.[1−10] Although extensive photophysical studies targeting improved understanding of the excited-state dynamics of optical detection that exploit specific probes have been performed,[9−12] the search for novel, controllable, and tunable probe molecules is still a promising task.[1]

In this context, the benzo[*b*]quinolizinium (**BQ**) fluorophore has been established as a robust platform for the development of fluorescent probes with largely variable substitution patterns, as demonstrated with several examples of the selective fluorometric detection of pH, cations such as Hg^{2+} and Mg^{2+}, and biomacromolecules such as nucleic acids and proteins.[13−21] Recently, 9-aryl-substituted **BQ** derivatives were demonstrated to display moderate fluorescence quantum yields, except for 9-(*p*-*N*,*N*-dimethylaminophenyl)-**BQ** (**1**)[22] (Scheme 1), which was essentially nonemissive [ϕ_{fl} (**1**) < 0.001]. Protonation of the amino functionality to afford the dimethylammoniophenyl analogue **2**, however, gave rise to a strong emission light-up effect. Unraveling the atomistic details of this highly effective turn-on functionality will be illuminating in designing similarly functioning light-up probes. In particular, why **1** assumes a nonemissive excited state and how the nonradiative deactivation takes place remain unknown. Moreover, the existence of deactivation channels other than fluorescence for **2** needs clarification, since the pH-triggered fluorescence quantum yield did not reach unity [ϕ_{fl} (**2**) = 0.14].

Scheme 1. Structure and Numbering of 1 and Its Conversion to 2 by Protonation of the Amine Nitrogen (N^a)[23]

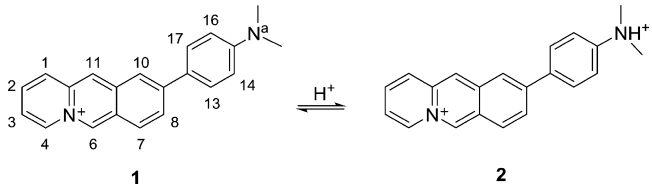

The details of the electronic structure of this system may serve as a general model for comprehending the pH-responsive fluorescence light-up effect in aryl-substituted cationic aromatic species and may lead to a significantly improved understanding of the excited-state dynamics of potent optical probes. Although examples of pH-sensitive fluorescent light-up probes

Received: December 12, 2013
Published: April 8, 2014

   dx.doi.org/10.1021/jo402756y | *J. Org. Chem.* 2014, 79, 3799−3808

are common,[24−30] the fine details of the underlying photophysics from a thorough theoretical perspective, which will assist rational design strategies, are missing. Therefore, in order to establish general principles, we here corroborated the excited-state properties and electronic structure details for species **1** as well as the changes accompanying protonation to afford **2**. Extensive comparison of the low-lying electronic states of **1** and **2** by means of quantum-chemical modeling using state of the art CASSCF,[31,32] CASSCF-MP2,[33,34] DFT,[35,36] and TD-DFT[37] techniques was carried out. Furthermore, insights based on key electronic structure fingerprints of **1** and **2** were utilized to construct model systems for which excited-state analyses successfully demonstrated that in silico design of new light-up probes is a promising path.

RESULTS AND DISCUSSION

Selected structural parameters (Å, deg) for the optimized ground states of **1** and **2** are given in Figure 1. Upon

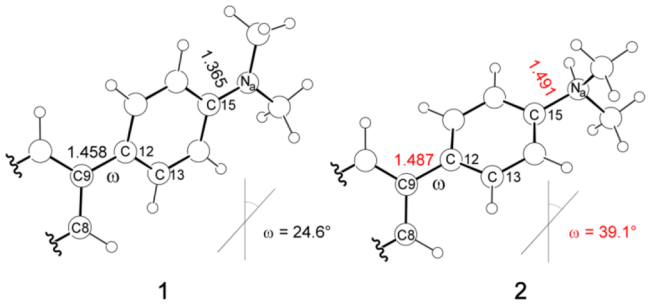

Figure 1. Selected structural parameters (Å, deg) of the ground-state geometries of **1** and **2** at the UB3LYP/6-31G(d,p) level of theory (ω is the C8−C9−C12−C13 dihedral angle).

protonation of N^a, the C15−N^a bond length increases by 0.13 Å, in line with a transition from an sp^2- to sp^3-hybridized nitrogen. Protonation also increases (i) the C9−C12 bond length by a small yet significant 0.03 Å as well as (ii) the C8−C9−C12−C13 dihedral angle between the two rings (ω) by 15°. These structural changes together point out decreased electronic communication between the two rings in the protonated state and can simply be attributed to the repulsion between the cationic **BQ** and the newly positively charged ammoniophenyl ring. The electronic structures of **1** and **2** are drastically affected by these perturbations (vide infra).

The contrasting luminescent behavior of **1** and **2** (as a result of protonation of the amine moiety) is a hint of the involvement of the N^a lone pair in the excitation process. This anticipation is verified by the molecular orbital analysis depicted in Figure 2.

In the case of **1**, the spatial distribution of the HOMO, which resides on the aminophenyl substituent with a substantial contribution from the nitrogen lone pair, and the LUMO, which is composed of the π system of the **BQ** fragment, suggest that an $S_0 \rightarrow S_1$ excitation of the HOMO → LUMO type yields a charge transfer (CT) from the aminophenyl ring to the **BQ** ring. Considering the extent of the nitrogen lone pair contribution to the HOMO (Table S1 in the Supporting Information), the character of this excitation can be termed as an n → π^* type of CT transition (Table S2).[38]

Once this n → π^* character is realized, it immediately follows that, the N^a−H σ bond (newly formed upon protonation) will drastically lower the energy of the N^a lone pair that was

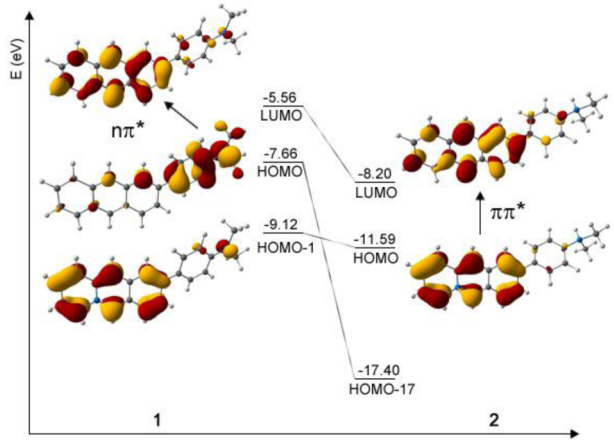

Figure 2. Frontier MO plots and energies (in eV) for **1** and **2** at the UB3LYP/6-31G(d,p) level of theory.

involved in the CT excitation. Thus, the corresponding N^a lone pair, which used to be the HOMO in **1**, will experience a huge decrease in energy and hence will no longer survive as a high-lying orbital in **2**. This presumed correlation is calculated to occur between the HOMO (at −7.66 eV) in **1** and the HOMO−17 (at −17.40 eV) in **2**.[39]

Comparison of the frontier orbitals also reveals that the domain of the excitation is different for the protonated species. Whereas the aminophenyl group in **1** behaves as the electron donor (ED) and the cationic **BQ** ring as the electron acceptor (EA), the fact that the HOMO and LUMO both reside on the π system of the **BQ** moiety in **2** gives rise to a $\pi \rightarrow \pi^*$ type of excitation. In other words, the $S_0 \rightarrow S_1$ excitation for **1** can be defined as an ED → EA type of CT transition, while **2** is locally excited in the **BQ** π system. Altering the absorption character in this fashion was possible through the electronic decoupling of the phenyl ring from the **BQ** chromophore in **2**. Thus, the neutral aminophenyl "donor" was converted into the cationic ammoniophenyl "spectator". Analysis of the electrostatic potential charge on the ED and EA rings as well as the orientation of the dipole moments also support this view (Table S3 and Figure S1).

The above rationale is supported by single-configuration TD-DFT calculations (Table S4) as well as by multiconfigurational CASSCF results (Figure 3). The distribution of the HOMO of **1** shows that the trigonal-planar orientation of the amino group positions the $2p_z$ atomic orbital of N^a, occupied by the lone pair, in a suitable symmetry for π-framework overlap with the phenyl moiety, suggesting that there is a large contribution to the HOMO from the N^a lone pair (also see Tables S1 and S2). Thus, the primary constituent of the $S_0 \rightarrow S_1$ excitation is an ED → EA type of CT from the aminophenyl moiety to **BQ**. Although the reliability of single-configuration methods may be questioned in the case of CT-type excitations, the TD-DFT results agree with the insight obtained from MO analysis of the ground states as well as the more reliable CASSCF results for the excited states, particularly for the CT character of the excitation. It should be noted that relying solely on TD-DFT results might be error-prone for the excitation energies of CT states.[40−43] The Coulomb-attenuated CAM-B3LYP[44] results (Table S4), however, are in good agreement with the experimental absorption energies for the CT transitions. It is noteworthy that our results clarify the key principles of designing pH-triggered fluorescence turn-on probes: the

dx.doi.org/10.1021/jo402756y | J. Org. Chem. 2014, 79, 3799−3808

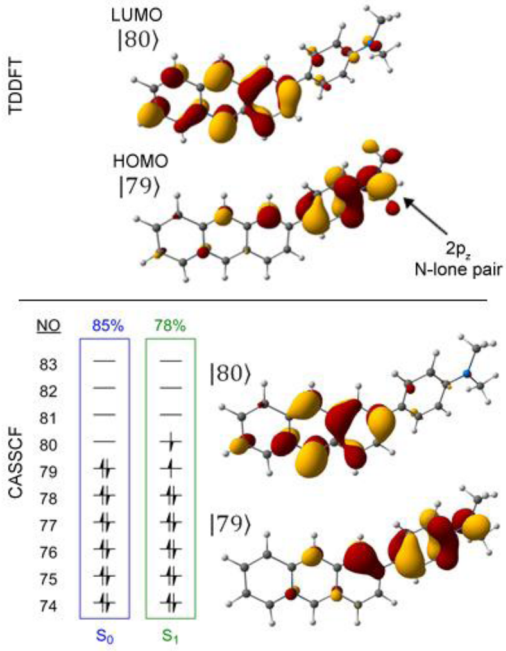

Figure 3. $S_0 \rightarrow S_1$ excitation character for **1**. (top) TD-DFT MO plots for the major transition. (bottom) Major configurations and natural orbital (NO) plots of CASSCF wave functions.

presence of an electron-deficient acceptor ring by virtue of a formally positively charged heteroatom and the existence of a suitable lone pair for donation seem essential. Applications employing similar approaches also support this view.[24−30]

The aforementioned structural and electronic properties of the ED and EA rings clarify the different emissive behaviors of **1** and **2** but do not seem to provide any clue concerning the dynamics of nonemissive deactivation of **1** on the excited-state surface. Further investigations of the low-lying excited states addressed this issue.

Experimentally, the emission of similar **BQ** derivatives was restored in highly viscous media such as glycerol without decreasing the pH.[15,19] Along the same line, the significant change in the computed dihedral angle ω, which defines the rotation of the aminophenyl ring with respect to the **BQ** ring, in going from **1** to **2** indicates that conformational change might play a critical role in the photophysics under investigation. The ED−EA ring rotation coordinate ω was identified to be the most important structural change by comparison of the S_0, S_1, and T_1 geometries for the two species (Tables S5−S7 and Figures S2−S4), and the evolution of the low-lying singlet and triplet states S_0, S_1, S_2, T_1, and T_2 along ω verified that inter-ring rotation is decisive in the relative spacing of the states (Figure S5). The path most relevant to the deactivation, however, is the migration from the FC point to the S_1 equilibrium structure. The relative energies of the S_1 states of **1** and **2** along this FC $\rightarrow$ S_1 equilibrium coordinate (with all internal coordinates allowed to change) are depicted in Figure 4c,d (also see Table S8).

The barrier of ca. 0.4 eV shown in Figure 4c suggests that the S_1 equilibrium might not be reachable. However, such a barrier can exist when coordinates interpolated between the FC and S_1 geometries are used, and a dissection of the important changes along the FC $\rightarrow$ S_1 vector is required (Figure 4e and Table S10).[45] Similar analyses of excited-state relaxation paths by using the two most important coordinates were previously employed,[46,47] but mainly in the context of spin-allowed nonradiative deactivation. It is natural to assume that the ring rotation coordinate ω(C8−C9−C12−C13) and the inter-ring separation coordinate R(C9−C12) provide relaxation paths on the S_1 surface. However, inspection of the changes in all of the internal coordinates reveal that ω(C8−C9−C12−C13) and the phenyl−amine bond length R(C15−N^a) are the two significant changes along the FC $\rightarrow$ S_1 vector. R(C9−C12) is essentially unchanged, with a mere 0.5% increase from 1.479 Å at the FC point to 1.486 Å at S_1. Nevertheless, elongation of R(C9−C12) up to 2.000 Å is also shown to be uphill on the S_1 surface (Figures S7 and S8 and Tables S11 and S12). Decoupling of the FC $\rightarrow$ S_1 vector into the primary components ω and R(C15−N^a), as depicted in Figure 4e, suggests that the C15−N^a contraction is essentially barrierless and the inter-ring rotation costs only 0.15 eV. Thus, if the FC $\rightarrow$ S_1 decay path primarily follows the two uncoupled coordinates, the barrier height is lowered substantially from 0.4 eV via point A to 0.2 eV via point B. After point B is reached at 2.76 eV, a shallow S_1 surface is experienced until the S_1 equilibrium is reached. Given the experimental observations on ISC of similar **BQ** derivatives,[21] the existence of a barrier along all three FC $\rightarrow$ S_1 decay paths (Figure 4e) is questionable.

Our final analysis of the energetics of the decay mechanism of **1** utilized the FC $\rightarrow$ S_1 full relaxation path, where gradients on the S_1 surface are calculated (Figure 4f and Table S13). All of the points lie below the FC energy, so this FC $\rightarrow$ S_1 minimum-energy path (MEP) can allow the S_1 wave packet to access the S_1 equilibrium geometry. The most important features of the MEP are the following: (i) the major reaction coordinate on the MEP is ω; (ii) the path is very shallow; and (iii) the S_1 and T_1 surfaces are near degenerate along all of the surface. The slight 0.18 eV dive experienced initially does not yield an energy minimum on the S_1 surface because of nonzero forces. After a vertical (89.2°) alignment of the rings is achieved, the forces tend to zero, and that portion of the MEP is extremely flat. A vanishing singlet−triplet energy gap even at limited regions of the excited-state surface has been reported to yield facile ISC.[48] Besides, near degeneracy on a large portion of the decay path was recently shown to induce unexpectedly high yields of ISC despite very small spin−orbit coupling constants.[49,50] Moreover, there is no support for a spin-allowed deactivation of **1**, as we did not encounter any portions of the excited-state potential energy surface approaching the ground state along any of the coordinates screened (Figures S6−S8 and Tables S10 and S13). The S_1−S_0 separation always remained large. All of the above findings as well as the experimental evidence suggest that **1** undergoes fast $S_1 \rightarrow T_1$ ISC along the FC $\rightarrow$ S_1 MEP, where the S_1 and T_1 states are always near degenerate. We should note that it is not possible to quantify the fraction of the excited-state wave packet that ends up on the triplet surface. These results may be available from excited-state quantum dynamics studies that are beyond the scope of the current work.

On the other hand, **2** experiences a downhill energy surface from the FC region to the S_1 equilibrium geometry where fluorescence emission takes place. This energy- and spin-allowed process is likely to drive the excited singlet wave packet toward the S_1 equilibrium before interference with any other spin-forbidden processes (see Tables S8 and S9 for all values). The other requirement for efficient ISC is an electronic match of the wave functions among the different spin states (vide infra).[51−53]

dx.doi.org/10.1021/jo402756y | J. Org. Chem. 2014, 79, 3799−3808

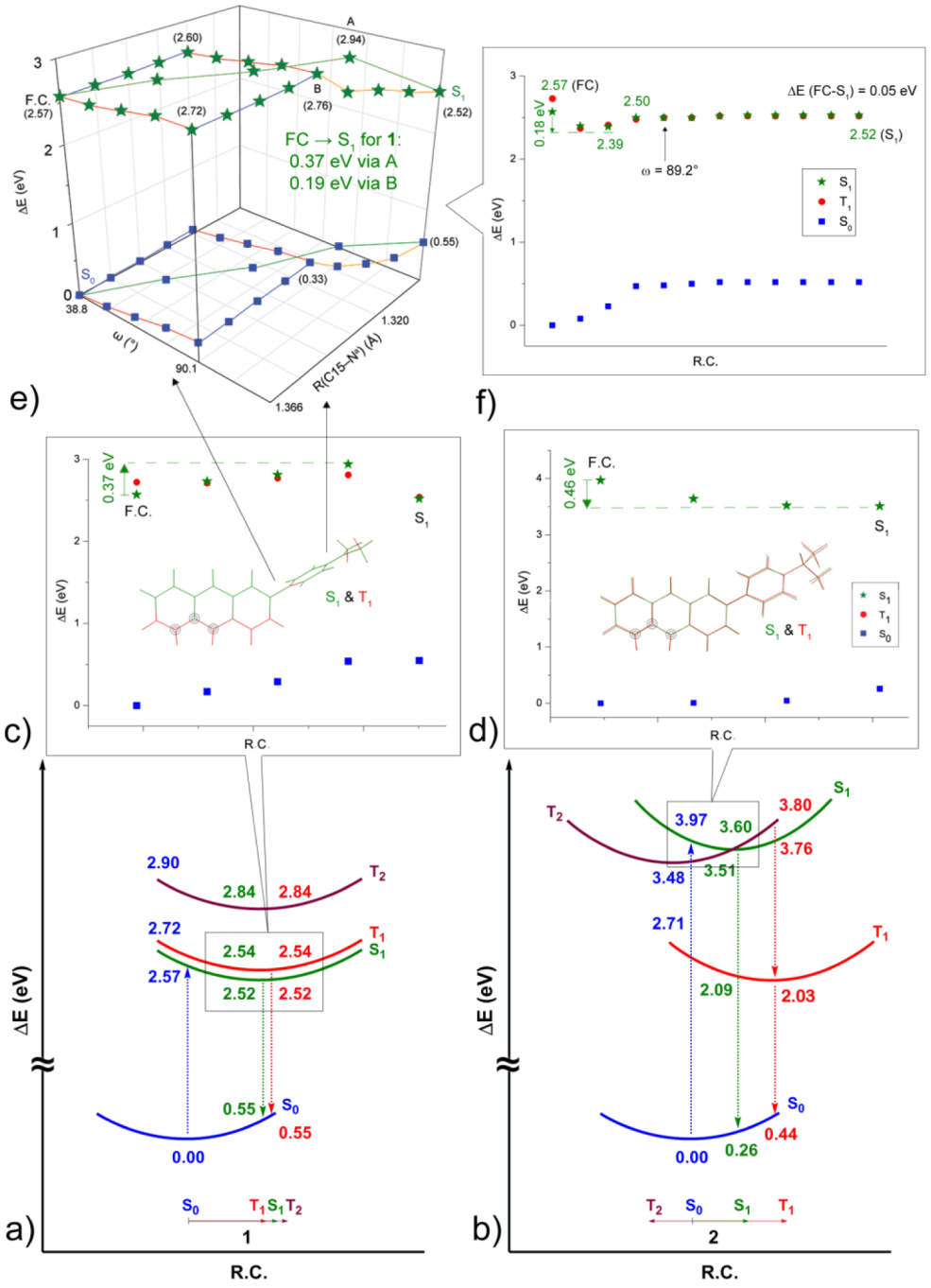

Figure 4. (a, b) Relative energies of all possible vertical and adiabatic transitions for **1** and **2** at the CASPT2(12,10)/6-31G(d,p) level of theory (also see Table S9). (c, d) Relative energies of the S_0 and S_1 states along the FC → S_1 coordinate. The T_1 state, which is near degenerate with S_1, is also shown for **1**. The T_1 state of **2** always lies well below S_1. The S_1–S_0 separations for both species are always large and do not indicate any spin-allowed nonradiative deactivation of the S_1 states. Superimposed equilibrium structures of S_1 and T_1 states are also given. Tether points are shown with circles. (e) Relative energies of the S_0 and S_1 states along the FC → S_1 coordinate via ring rotation (ω) and along the C15–N^a bond for **1** (the T_1 surface has been excluded for clarity; see Figure S6 and Table S10). After the changes in ω and C15–N^a are applied (at point B), there are still minor differences with the S_1 geometry, and the points from B to S_1 account for those minor changes. (f) Relative energies of the S_0, T_1, and S_1 states along the FC → S_1 minimum-energy path (MEP) for **1**.

The vertical and adiabatic transitions depicted in Figure 4 show that **2** does not possess a near degenerate S_1–T_1 pair, contrary to **1**. S_1 and T_1 are separated by 1.5 eV, a large difference that could originate from drastically different electronic structures of the S_1 and T_1 states of **2**. On the other hand, not identical but comparable to the S_1–T_1 near degeneracy of **1**, there is an S_1–T_2 near degeneracy in **2**. Therefore, the possibility of an S_1 → T_2 hop for **2** should be investigated. Details of the electronic structures of the S_1, T_1, and T_2 states are enlightening in that respect and are given in Figure 5. These multiconfigurational wave functions and plots of the important natural orbitals (NOs) allow us to draw qualitative descriptions of all the electronic states under investigation.

Both species possess a closed-shell ground state, and the S_2 states lie too high in energy to be relevant to the luminescent

dx.doi.org/10.1021/jo402756y | J. Org. Chem. 2014, 79, 3799–3808

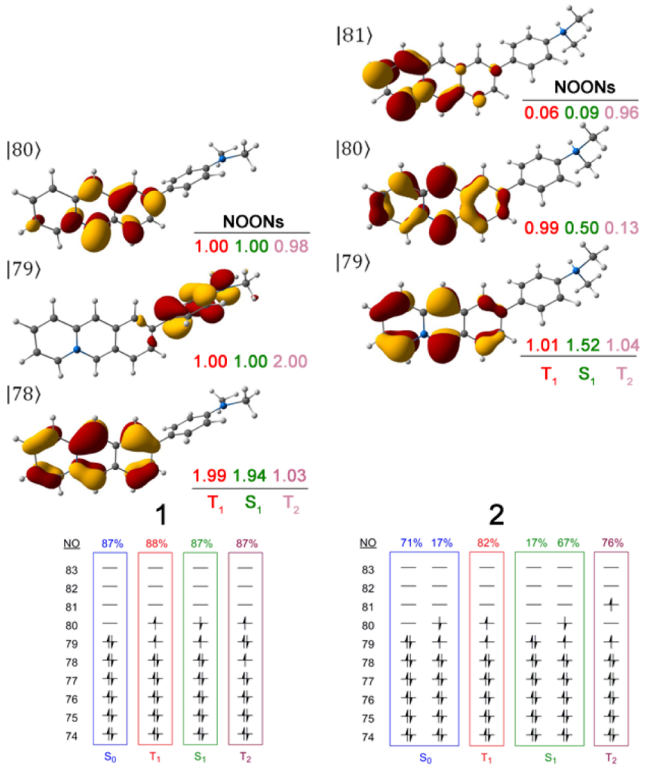

Figure 5. Details of the wave functions, natural orbital occupation numbers (NOONs), and NO plots for **1** and **2**. For both species, S_0 and S_1 state-averaged CASSCF wave functions were computed at the S_1 equilibrium geometry, and the T_1 and T_2 states were computed at the T_1 equilibrium geometry. Orbitals are plotted at the S_1 equilibrium geometry for **1** and the T_1 equilibrium geometry for **2**.

behavior (Figure S5). For the T_1 states of both species, natural orbital occupation numbers (NOONs) show a pair of highest-lying singly occupied orbitals (i.e., the typical first triplet state). On the other hand, there is a critical difference in the spatial domains of these singly occupied orbitals. While orbitals ED-79 and EA-80, confined to the respective electron donor and electron acceptor, are used to construct the simplified T_1 wave function for **1**,

$$T_1(\mathbf{1}) \approx |[\text{closed shell}]\phi_{\text{ED-79}(\uparrow)}\phi_{\text{EA-80}(\uparrow)}| \quad (1)$$

the singly occupied orbitals for the T_1 state of **2** both reside on the **BQ** moiety (which used to be the EA in **1**). Thus, the corresponding simplified T_1 wave function for **2** can be written as

$$T_1(\mathbf{2}) \approx |[\text{closed shell}]\phi_{\text{EA-79}(\uparrow)}\phi_{\text{EA-80}(\uparrow)}| \quad (2)$$

The S_1 wave functions for these two species also show similar configurational motifs, namely,

$$S_1(\mathbf{1}) \approx |[\text{closed shell}]\phi_{\text{ED-79}(\uparrow)}\phi_{\text{EA-80}(\downarrow)}| \quad (3)$$

and

$$S_1(\mathbf{2}) \approx |[\text{closed shell}]\phi_{\text{EA-79}(\uparrow)}\phi_{\text{EA-80}(\downarrow)}| \quad (4)$$

However, the S_1 state of **2** possesses significant multiconfigurational character that renders the assignment in eq 4 incomplete (Table S14). In view of the inherent complexity of any molecular wave function (even in the ground state), the simplifications presented herein are unavoidable if a conceptual framework is sought. Thus, we utilized the simplified wave functions summarized in Table 1 for a tractable conceptual description and comparison of the excited state wave functions.

Table 1. Simplified Wave Functions[a] of the S_0, T_1, S_1, and T_2 States of 1 and 2

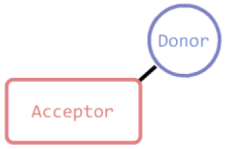

state	1	2
T_2	$\lvert\phi_{\text{EA-78}(\uparrow)}\phi_{\text{EA-80}(\uparrow)}\rvert$	$\lvert\phi_{\text{EA-79}(\uparrow)}\phi_{\text{EA-81}(\uparrow)}\rvert$
S_1	$\lvert\phi_{\text{ED-79}(\uparrow)}\phi_{\text{EA-80}(\downarrow)}\rvert$	$\lvert\phi_{\text{EA-79}(\uparrow)}\phi_{\text{EA-80}(\downarrow)}\rvert$
T_1	$\lvert\phi_{\text{ED-79}(\uparrow)}\phi_{\text{EA-80}(\uparrow)}\rvert$	$\lvert\phi_{\text{EA-79}(\uparrow)}\phi_{\text{EA-80}(\uparrow)}\rvert$
S_0	$\lvert\phi_{\text{ED-79}(\uparrow)}\phi_{\text{ED-79}(\downarrow)}\rvert$	$\lvert\phi_{\text{EA-79}(\uparrow)}\phi_{\text{EA-79}(\downarrow)}\rvert$

[a]ED denotes the electron donor ring and EA the electron acceptor ring. ϕ_{EA} denotes an orbital mainly confined to the A ring and ϕ_{ED} an orbital mainly confined to the D ring. Minor contributions to the multiconfigurational wave functions have been excluded for clarity.

Although the unpaired electrons of the T_1 and S_1 states occupy the two highest-lying orbitals (ϕ_{79} and ϕ_{80}), giving rise to typical T_1 and open-shell S_1 states for both **1** and **2**,[54] the different luminescent behaviors can be rationalized on the basis of the general rules for ISC outlined by Salem[55,56] and Shaik[57−59] for **1**. From an electronic structure point of view, the CT nature of S_1 of **1** and the twisted alignment of the two singly occupied MOs enhance the probability of surface crossing to the triplet surface. (Energy considerations are given in the discussion of Figure 4.) This rationale is supported experimentally by verification of ISC for other **BQ** derivatives,[21] although phosphorescence of **1** could not be determined in solution at room temperature.

In case of **2**, on the other hand, it is important to corroborate why $S_1 \rightarrow T_1$ ISC cannot be invoked. First, the large energy difference between the S_1 and T_1 states of **2** has already been mentioned. This gap is due to quantum-mechanical exchange, which stabilizes a triplet state $|\varphi_1(\uparrow)\varphi_2(\uparrow)|$ with respect to an open-shell singlet state $|\varphi_1(\uparrow)\varphi_2(\downarrow)|$, where wave functions for both states are built from the same pair of orbitals φ_1 and φ_2.[60] Consequently, the T_1 wave function of **2**, which is generated from orbitals local to a single spatial domain (i.e., the EA **BQ** π system), experiences favorable exchange interactions that scale with the phenomenological exchange term:

$$\langle\phi_{\text{EA-79}(\uparrow)}\phi_{\text{EA-80}(\uparrow)}|\phi_{\text{EA-80}(\uparrow)}\phi_{\text{EA-79}(\uparrow)}\rangle$$

On the other hand, the ED and EA rings are spatially orthogonal to each other in the case of **1**, and the two unpaired electrons in the triplet state, which reside in distinct and nonoverlapping orbitals, are not amenable to an appreciable amount of exchange. Hence, quantum-mechanical exchange stabilization, which generally yields the energetic ordering $S_0 < T_1 < S_1$, does not contribute to energy lowering of T_1 in the case of **1**. Therefore, the S_1 and T_1 states of **1** are near degenerate along the inter-ring rotation coordinate. Consequently, the contrasting luminescence properties of **1** and **2**, realized as a delicately adjusted S_1−T_1 gap, originate from central electronic structure differences in the construction of the excited states. This is a critical understanding that enables

dx.doi.org/10.1021/jo402756y | J. Org. Chem. 2014, 79, 3799−3808

one to pave the way to rational design, since the "whys" and "why nots" of the observed photophysics have been clarified.

At this point, one should wonder why the same principles do not hold for the S_1 and T_2 states of **2**. First, we can invoke the general ISC rules outlined by El-Sayed,[61,62] as both the $S_1 \rightarrow T_1$ and $S_1 \rightarrow T_2$ transitions are among states of the $\pi \rightarrow \pi^*$ type. According to El-Sayed, such transitions are forbidden. CASSCF wave functions and NOs also supports this view as NOs $|79\rangle$, $|80\rangle$, and $|81\rangle$ all lie in the π framework of BQ and hence do not supply the angular momentum change that must be associated with a spin inversion (i.e., there is no change in the orientation of the orbitals). When the presence of different cases for ISC as nicely summarized by Caldwell[63] is noted, the El-Sayed rules perfectly apply to **2**, but **1** requires the treatment of Salem and Rowland since the excitation is between the two constituents of a twisted chromophore. In addition, a better match with the highly multiconfigurational wave functions of the S_0 and S_1 states of **2** and the lack of such a similarity for **1** are also notable in rationalizing the fluorescence of **2**.

Estimation of ISC probabilities is also possible via the Landau–Zener[64] (LZ) treatment. However, as clearly noted by Danovich and Shaik,[51] one should not dwell on the numerical values calculated by the LZ approach. Two critical parameters in estimating ISC probabilities are (*i*) the magnitudes of the spin–orbit coupling constants (SOCCs), which account for the compatibility of the wave functions of the two different spin states, and (*ii*) the energy difference between the electronic states. Because of the many approximations involved in computing the SOCCs and using the approximate LZ treatment,[65] our results should be treated as semiquantitative at best. The ISC probabilities, which scale with the second power of the SOC matrix element and are inversely proportional to the square root of the energy gap, yield a ca. 64-fold rate difference for singlet–triplet hopping for **1** over **2** with orthogonal arrangement of the ED and EA rings, where the S_1–T_1 SOCCs for **1** and **2** are 3.86 and 0.89 cm^{-1}, respectively (see Table S15 for the evolution of the relative ISC rates along the ring rotation coordinate).[66]

Although $S_1 \rightarrow T_1$ as well as $S_1 \rightarrow T_2$ ISC for **2** is forbidden according to El-Sayed's rules, we calculated "small" but not vanishing SOCCs for the $S_1 \rightarrow T_1$ transition, but the $S_1 \rightarrow T_2$ SOCCs vanished. We speculate that compatibility with respect to a spin flip, as recently utilized by Dede at al.[53] for ISC phenomena, is an alternative explanation for this observation. That is, a simple spin flip in the S_1 state of **2** does not yield the T_2 wave function but instead converts the S_1 configuration $|\phi_{EA\text{-}79(\uparrow)}\phi_{EA\text{-}80(\downarrow)}|$ to $|\phi_{EA\text{-}79(\uparrow)}\phi_{EA\text{-}80(\uparrow)}|$, which indeed defines the T_1 state. It should be noted that the topology and energetics of the S_1 surface seem to surpass the effect of ISC for **2** since the FC $\rightarrow S_1$ decay is barrierless.

Although fluorescence emission from the S_1 state of **2** is understood on the basis of an electronically well-protected[67] (i.e., ISC-resistant) singlet excited state, the emission quantum yield is low. This can be attributed to the fact that motion along the ring rotation coordinate has only a slight energetic penalty. As shown in Figure S9, full rotation on the S_1 surface costs 0.12 eV. Thus, even if a large degree of dissipation of the excess energy at the FC state (0.46 eV) to the surroundings is assumed, the ammoniophenyl ring of **2** can be granted full rotation with only one-fourth of this excess energy (see Table S16). Although it is not possible to quantify the amount of excess energy dissipated to the solvent medium as well as the exact loss of emissive power due to rotational relaxation, the near-unity fluorescent quantum yields in viscous media[15,19] suggest that phenyl rotation is essentially free and deactivates a significant amount of the excited-state wave packet non-radiatively. The excited-state wave packet of **1** behaves similarly along the rotational deactivation channel. These results point out retardation of the ammoniophenyl rotation as a synthetic direction in increasing the emission quantum yield, which can be achieved by incorporating substituents on carbon atoms 8, 10, 13, and 17. Similar approaches have been utilized for twisted intermolecular CT systems.[68]

The insight obtained from the analysis of wave functions, CASSCF natural orbitals, and occupancies can find practical uses in the design and investigation of luminescent properties of ED–EA systems similar to **1** and **2**. In order to demonstrate that our concept-driven theoretical analysis is useful for this purpose, we constructed the model systems depicted in Chart 1. In particular, the presence of the donor amine moiety and

Chart 1

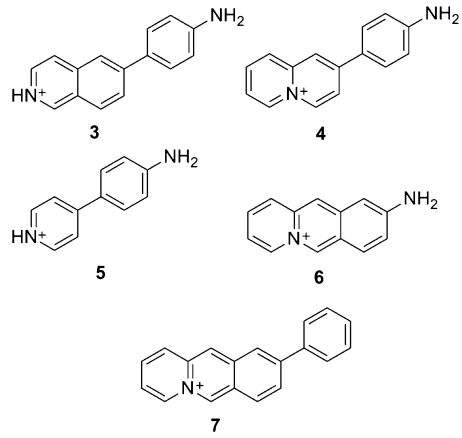

phenyl spacer as well as the size of the acceptor ring were used as control parameters in order to understand the effect of these emerging structural motifs of the **1**/**2** couple on the observed photophysics. Frontier orbital analyses of models **3**–**7** are helpful in corroborating the validity and extent of the basic principles of turn-on fluorescence observed for **1** and **2**. Table 2 gives the energy differences between the S_1 and T_1 states at different ring rotation angles, and Table 3 shows the singly occupied orbital plots for the S_1 states for the models.

Table 2. S_1–T_1 Energy Differences for the Model Systems in the Neutral (3–7) and Protonated (3H–6H) Forms at the CASPT2(6,6)/6-31G(d,p) Level of Theory

		$\Delta E(S_1\text{–}T_1)$ (eV)				
species	geometry	3	4	5	6	7
neutral (**n**)	S_0	0.58	0.62	0.81	0.72	1.02
	ω = 90°	0.04	0.11	0.13	N/A	N/A
protonated (***n*H**)	S_0	0.74	1.06	1.16	1.37	N/A

Similar to the energetic spacing of the S_1 and T_1 states for the **1**/**2** couple, orthogonal arrangement of the rings decreases the S_1–T_1 gap substantially. Above (see eqs 1–4), we have justified that significant CT character yields a narrow S_1–T_1 gap when the spatial domains of the two singly occupied orbitals are different and do not overlap to a significant extent. Following this argument, the low S_1–T_1 gaps with orthogonal arrange-

dx.doi.org/10.1021/jo402756y | J. Org. Chem. 2014, 79, 3799–3808

Table 3. Singly Occupied MO Plots of Model Systems[a]

Species	3	4	5	6	7
Neutral (n)	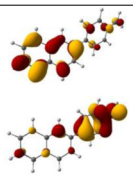	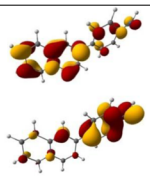	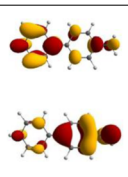	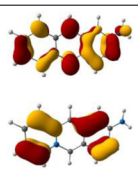	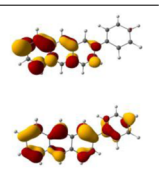
Protonated (nH)	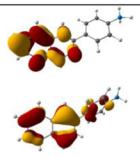	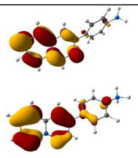	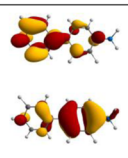	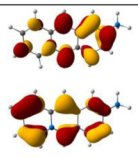	N/A

[a]Orbitals were selected by inspecting the major TD-DFT transitions. The singly occupied MOs were constructed from the ground-state electron density and hence represent the HOMO and LUMO for the S_0 state.

ment of the ED and EA rings calculated for **3**, **4**, and **5** suggest that the S_1 states of these species will have a favorable ISC channel for deactivation. For (aminophenyl)pyridinium **5**, existing experimental data[69] support both a negligible fluorescence quantum yield and a rotational deactivation mechanism. This is in line with our deductions from the low S_1-T_1 gap above and the orbital analysis discussed below. It should be noted that the S_1-T_1 gap for the protonated species increases because T_1 experiences a larger amount of exchange.

Table 3 shows the singly occupied orbitals making up the S_1 and T_1 states for the unprotonated and protonated model systems. Inspecting the confinement of the orbitals to the ED or EA rings is instructive in envisioning the fate of the excited state, but this analysis should not be treated conclusively as we do not present a full-scale exploration of the excited-state potential energy surfaces for the models.

When one of the singly occupied orbitals is mainly localized on the ED ring and the other on the EA ring, such as in the case of **3** and **4**, the energetic separation between the S_1 and T_1 states is small. This is due to the aforementioned lack of exchange in the T_1 state. When the EA ring is truncated to give **5**, charge separation between the ED and EA rings is not very efficient, as also indicated by the increased S_1-T_1 gap compared with **3** and **4**. On the other hand, the electron densities on the ED and EA rings are still well-preserved for **5**, suggesting a CT-type transition. The substantial nitrogen lone-pair contribution to HOMO of **5** should be noted. This observation is in line with the available experimental data,[69] and it also shows the importance of the size of the EA ring in effectively distributing the charge density. In another view, enlarging the model decreases the mixing of the two π systems on the ED and EA rings. Locality of quantum-mechanical exchange is an equivalent and alternative approach to explain this observation, as successfully employed in a similar problem recently.[52] Thus, in order to reproduce the photophysics of the **1**/**2** couple, the ED and EA rings should be large enough to break down exchange of electrons residing in the singly occupied orbitals. This rationale was further tested by increasing the separation between the ED and EA rings and analyzing the frontier orbitals as well as the S_1-T_1 SOCCs for **5** (Tables S17 and S18 and Figure S10). The larger the separation, the better-resolved are the donor and acceptor orbitals and the larger is the S_1-T_1 coupling.

When the amino group and the cationic EA ring are not separated by the aromatic spacer, as in the case of **6**, the lone pair of the amine nitrogen mixes with the π system of the **BQ** ring and does not possess an independent donor character. This gives rise to a local $\pi \rightarrow \pi^*$ type of transition on **BQ**, in excellent agreement with experimental emission measurements of 9-aminobenzo[*b*]quinolizinium derivatives without the phenyl spacer.[70] Finally, **7** shows the importance of the lone pair of the amine nitrogen for donation, as its absence shifts the singly occupied orbitals to the cationic EA ring once again to yield a $\pi \rightarrow \pi^*$ type of transition. The phenyl π system only slightly contributes to the HOMO, leaving a substantial amount of electron density on the EA ring. Thus, the phenyl ring alone cannot act as an electron donor (also see Tables S1 and S2).

Orbital analysis of the protonated models **3H**, **4H**, and **6H** suggests a locally excited $\pi \rightarrow \pi^*$ type of S_1 state on the EA ring, as shown in Table 3. While the fluorescence turn-on mechanism is anticipated for **3H** and **4H**, the photophysics of the **5**/**5H** and **6**/**6H** couples should be different from that of the **1**/**2** couple because of the absence of well-defined ED and EA frontier orbitals.

The results deduced from the orbital analysis above are also supported by the structural features of the models outlined in Table 4. For the protonated species **3H** through **6H**, the inter-ring dihedral angles as well as the C−C bond lengths connecting the rings increase. Consequently, the reduced electronic communication and decreased orbital overlap yield more twisted structures and afford locally excited states whose protonated forms can generally be described as

$$S_1(\mathbf{nH}) \approx |[\text{closed shell}]\phi_{\text{EA-HOMO}(\uparrow)}\phi_{\text{EA-LUMO}(\downarrow)}| \quad (5)$$

Table 4. Pertinent Structural Parameters of the Model Systems 3−7

species	inter-ring dihedral angle (deg)	inter-ring bond length (Å)
3	24.0	1.456
3H	40.3	1.488
4	20.5	1.453
4H	39.0	1.486
5	16.8	1.445
5H	38.1	1.486
6	N/A	1.352[a]
6H	N/A	1.493[a]
7	33.9	1.476

[a]C−N bond length.

dx.doi.org/10.1021/jo402756y | J. Org. Chem. 2014, 79, 3799−3808

for **3H**, **4H**, and **6H**.

The data summarized in Tables 2−4 show that the energy spacing of the S_1 and T_1 states, localization/delocalization of the frontier MOs, and structural perturbations of the inter-ring bond length and angle showing the degree of electronic communication between the two rings can be used as convenient parameters to assess the potential of twisted chromophores for a fluorescence turn-on action similar to that observed for the **1**/**2** couple. In addition, the structural and electronic analysis of the model systems is straightforward, as most of it relies on the DFT/TD-DFT results. Thus, it is possible for the nonexpert computational chemist to be guided by analogous calculations during the identification of synthetic targets. Similar ED−EA systems were successfully studied for CT excitation character using TD-DFT.[71,72] A thorough investigation of excited-state deactivation mechanisms of the models is beyond the scope of the current work and may fully be achieved by employing excited-state quantum dynamics methods.[73] Nevertheless, the models successfully demonstrate that the photophysics similar to that of **1**, that is, the nonemissive decay and pH-responsive fluorescence light-up effect can be reproduced by considering the design principles, which can be summarized as the presence of (i) a cationic acceptor larger than a single aromatic ring, (ii) a lone pair on a heteroatom as a Brønsted base, and (iii) a spacer ring between the ED lone pair and the EA ring.

CONCLUSION

Low-lying electronic states of 9-(4-*N*,*N*-dimethylaminophenyl)-benzo[*b*]quinolizinium (**1**) and similar model systems were investigated by quantum-chemical modeling employing state-of-the-art CASPT2 and TD-DFT techniques. Our results show that a donor → acceptor CT transition takes place in the excitation of aminophenylbenzo[*b*]quinolizinium. $S_1 \rightarrow T_1$ ISC enhanced by the near degeneracy of these electronic surfaces is suggested to largely contribute to excited-state deactivation.

The same principles do not operate for the protonated form of the molecule, as the protonated ring is no longer able to donate electrons, giving rise to the locally excited S_1 state on the acceptor benzo[*b*]quinolizinium ring. The spin-allowed FC → S_1 decay is calculated to be downhill. The local triplet state experiences large amount of quantum-mechanical exchange that stabilizes it and prevents it from lying close to S_1, rendering the ISC channel inaccessible. The close-lying T_2 state cannot be accessed because $S_1 \rightarrow T_2$ ISC is forbidden according to the El-Sayed rules.

The nonemissive character of the unprotonated form and the fluorescence turn on can simply be summarized as shown in Scheme 2: (i) transformation of a donor lone pair to a σ bond via protonation; (ii) switch of the nonlocal donor → acceptor character of the $S_0 \rightarrow S_1$ excitation to afford a local acceptor → acceptor character; (iii) stabilization of T_1 due to favorable quantum-mechanical exchange interactions among the singly occupied same-spin orbitals confined to the acceptor ring; (iv) creation of a large S_1-T_1 energy gap due to the stabilized T_1 state; (v) recovery of fluorescence emission as S_1 is rapidly accessed from the FC point and other deactivation pathways are electronically forbidden.

Scheme 2. Summary of the CT Turn-Off and Fluorescence Light-Up Effect

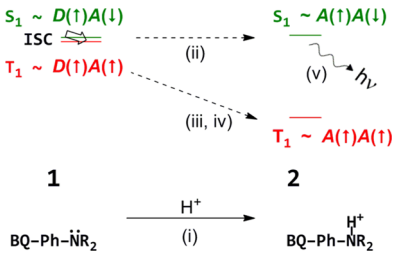

Model systems supported the insight obtained from the electronic structure analysis on (amino/ammoniophenyl)-acridizinium and nicely demonstrated the predictive power of our orbital interpretation. Available photophysical data verified our predictions based on simple yet powerful molecular orbital arguments. We believe that the principles outlined in this work can help in the design of pH-controlled fluorescence turn-on probes with well-defined donor and acceptor sites having desired luminescence properties.

COMPUTATIONAL DETAILS

Geometry optimizations were performed using the ab initio complete-active-space self-consistent field (CASSCF)[31,32] technique and density functional theory (DFT)[35,36] with the B3LYP[74−79] hybrid functional. Pople's all-electron double-ζ basis including d- and p-type polarization functions was used considering its reliable performance in excited states of similar organic chromophores and computational feasibility.[52,67,80] Dunning's correlation-consistent triple-ζ cc-pVTZ[81] basis was used for single-point energy refinements of the TD-DFT results. Harmonic vibrational frequencies were computed to verify that the species were true minima (i.e., none of the eigenvalues of the Hessian matrix were negative). TD-DFT calculations in combination with a polarizable continuum model (PCM)[82,83] employing solvent parameters of acetonitrile and water were performed to investigate the excitation characteristics of **1** and **2**. Solvents were selected to match the experimental absorption and emission measurements.[22] TD-DFT calculations on **1** and **2** were also performed utilizing the Coulomb-attenuated functional CAM-B3LYP.[44]

The active spaces in the CASSCF calculations were chosen from the highest-lying π and π^* orbitals obtained as the eigenvectors of the Kohn−Sham DFT calculations (Tables S19−S23). Plots of all of the active orbitals constituting the 12,10 active space for **1** and **2** and the 6,6 active space for the model species **3**−**7** are given in Tables S24−S30. An 8,7 active space was sometimes used to provide an initial guess for the 12,10 calculations when convergence problems were encountered with the 12,10 active space. NOs and NOONs were monitored to assure the desired active space convergence in the CASSCF calculations. NOs are the most convenient way to build the MCSCF wave function, as they provide the shortest expansion in the configuration space. NOONs are the diagonal elements of the one-electron density matrix having nonintegral values from 0 to 2. The analyses of wave functions given in Figures 3 and 5 show the NOONs and weight (square of the configuration state function coefficient) of the displayed configuration in the multireference expansion. Perturbation corrections to the CASSCF results were performed using Roos' CASPT2 method.[33,34] Exploratory runs showed that no level shifting was required for the CASPT2 calculations. Excited-state calculations employed the state-averaged[84] formalism, where the states of interest were computed with equal weights. Singlet and triplet states were treated separately in the state-averaging formalism. Figures S11 and S12 display selected structural parameters for **1** and **2** optimized at various levels of theory.

FC → S_1 reaction coordinates were probed for **1** and **2** by gradually transforming the internal coordinates at the vertically excited Franck−Condon point into S_1 equilibrium structures. Rotational barriers on the S_1 surfaces of **1** and **2** were studied at the optimized S_1 geometries and varying the inter-ring dihedral angle ω at the CASPT2(12,10)/6-31G(d,p) level of theory (Figure S9 and Table S16). S_0 states for both species were also simultaneously studied in order to see the presence of any S_0-S_1 intersection region. At all times the S_0-S_1 separations

dx.doi.org/10.1021/jo402756y | J. Org. Chem. 2014, 79, 3799−3808

were greater than 2 eV. **5** and **5H** were subjected to a computational experiment to show that ED and EA sites of **5** are resolved upon increasing the inter-ring distance (Figure S10 and Tables S17 and S18). The inter-ring distances were elongated using 0.5 Å increments starting from the S_0 geometry at the CAS(4,4)/CEP-31G level of theory.

SOCCs were calculated by studying the nonadiabatic coupling of the singlet and triplet states using the Pauli−Breit Hamiltonian including both one-electron and two-electron terms.[85−87] The ratio of ISC probabilities for **1** and **2** was estimated by using the double-passage Landau−Zener nonadiabatic transition probability, which scales with the square of the SOC matrix elements and is inversely proportional to the square root of the energy spacing between the states of interest.[64,88] Details of the ISC treatment are given on pp S14−S15 in the Supporting Information.

Calculations were carried out with the MOLCAS 7.6,[89,90] GAMESS-US (version June 2013),[91] and Gaussian 03[92] software suites. The unprotonated species are labeled with numbers **1** to **7** excluding **2**. When the amine nitrogen (designated as N^a) is protonated, a capital "**H**" is appended to the species label (e.g., **3H** is the protonated form of **3**). Although **2** is equivalent to **1H**, because of the extensive discussion on **1** and its protonated form, **2** instead of **1H** is the preferred label. The label of the amine proton N^a is unconventional but was employed to distinguish it from the quinolizinium nitrogen in the discussions. The configurational representations of electronic states such as those given in Figures 3 and 5, Table 1, and eqs 1−4 are not correct antisymmetrized wave functions. They are Hartree-product-like representations of the dominant configurations utilized for illustrative purposes.

■ ASSOCIATED CONTENT

Supporting Information

Additional computational results, absolute energies, Cartesian coordinates, and MO plots. This material is available free of charge via the Internet at http://pubs.acs.org.

■ AUTHOR INFORMATION

Corresponding Authors

*E-mail: ihmels@chemie.uni-siegen.de.

*E-mail: dede@gazi.edu.tr.

Notes

The authors declare no competing financial interest.

■ ACKNOWLEDGMENTS

We thank TUBITAK (110T647) for financial support. S.Y. thanks TUBITAK for a scholarship. We are grateful to TUBITAK ULAKBIM (TR-Grid Infrastructure) and to the Gazi University Physics Department (pizag cluster) for computing resources and to the Deutsche Forschungsgemeinschaft for financial support. L.T. thanks the University of Siegen for a Fellowship for Female Graduate Students. We thank Muhammed Buyuktemiz for his assistance with the excited-state calculations. Dr. Zeynel Seferoğlu is gratefully acknowledged for contributions to initiation of this research.

■ REFERENCES

(1) Stennett, E. M. S.; Ciuba, M. A.; Levitus, M. *Chem. Soc. Rev.* **2014**, *43*, 1057.

(2) Yuan, L.; Lin, W.; Zheng, K.; He, L.; Huang, W. *Chem. Soc. Rev.* **2013**, *42*, 622.

(3) Yang, Y.; Zhao, Q.; Feng, W.; Li, F. *Chem. Rev.* **2013**, *113*, 192.

(4) Vendrell, M.; Zhai, D.; Er, J. C.; Chang, Y.-T. *Chem. Rev.* **2012**, *112*, 4391.

(5) Shi, W.; Ma, H. *Chem. Commun.* **2012**, *48*, 8732.

(6) Du, J.; Hu, M.; Fan, J.; Peng, X. *Chem. Soc. Rev.* **2012**, *41*, 4511.

(7) Chan, J.; Dodani, S. C.; Chang, C. J. *Nat. Chem.* **2012**, *4*, 973.

(8) Kobayashi, H.; Ogawa, M.; Alford, R.; Choyke, P. L.; Urano, Y. *Chem. Rev.* **2010**, *110*, 2620.

(9) Demchenko, A. P. *Introduction to Fluorescence Sensing*; Springer: Berlin, 2009.

(10) Lakowicz, J. R. *Principles of Fluorescence Spectroscopy*, 3rd ed.; Springer: New York, 2006.

(11) Berezin, M. Y.; Achilefu, S. *Chem. Rev.* **2010**, *110*, 2641.

(12) Loura, L. M. S.; Ramalho, J. P. P. *Molecules* **2011**, *16*, 5437.

(13) Tian, M.; Ihmels, H.; Ye, S. *Org. Biomol. Chem.* **2012**, *10*, 3010.

(14) Tian, M.; Ihmels, H. *Eur. J. Org. Chem.* **2011**, 4145.

(15) Faulhaber, K.; Granzhan, A.; Ihmels, H.; Otto, D.; Thomas, L.; Wells, S. *Photochem. Photobiol. Sci.* **2011**, *10*, 1535.

(16) Tian, M.; Ihmels, H.; Brotz, E. *Dalton Trans.* **2010**, *39*, 8195.

(17) Tian, M.; Ihmels, H.; Benner, K. *Chem. Commun.* **2010**, *46*, 5719.

(18) Tian, M.; Ihmels, H. *Chem. Commun.* **2009**, 3175.

(19) Granzhan, A.; Ihmels, H.; Viola, G. *J. Am. Chem. Soc.* **2007**, *129*, 1254.

(20) Bortolozzi, R.; Ihmels, H.; Thomas, L.; Tian, M.; Viola, G. *Chem.—Eur. J.* **2013**, *19*, 8736.

(21) Bohne, C.; Faulhaber, K.; Giese, B.; Häfner, A.; Hofmann, A.; Ihmels, H.; Köhler, A.-K.; Perä, S.; Schneider, F.; Sheepwash, M. A. L. *J. Am. Chem. Soc.* **2005**, *127*, 76.

(22) Tian, M.; Ihmels, H. *Synthesis* **2009**, 4226.

(23) The amino nitrogen is intentionally labelled to allow a clear discussion of relevant properties.

(24) Han, J.; Burgess, K. *Chem. Rev.* **2010**, *110*, 2709.

(25) Jager, W. F.; Hammink, T. S.; van den Berg, O.; Grozema, F. C. *J. Org. Chem.* **2010**, *75*, 2169.

(26) Tolosa, J.; Solntsev, K. M.; Tolbert, L. M.; Bunz, U. H. F. *J. Org. Chem.* **2009**, *75*, 523.

(27) Hutt, J. T.; Jo, J.; Olasz, A.; Chen, C.-H.; Lee, D.; Aron, Z. D. *Org. Lett.* **2012**, *14*, 3162.

(28) Shen, P.; Xiao, S.; Zhan, X.; Zhang, W.; Chang, K.; Yang, C. *J. Phys. Org. Chem.* **2013**, *26*, 858.

(29) He, H.; Ng, D. K. P. *Org. Biomol. Chem.* **2011**, *9*, 2610.

(30) Higginbotham, H. F.; Cox, R. P.; Sandanayake, S.; Graystone, B. A.; Langford, S. J.; Bell, T. D. M. *Chem. Commun.* **2013**, *49*, 5061.

(31) Schmidt, M. W.; Gordon, M. S. *Annu. Rev. Phys. Chem.* **2003**, *49*, 233.

(32) Roos, B. O. *Adv. Chem. Phys.* **1987**, *69*, 399.

(33) Andersson, K.; Malmqvist, P. A.; Roos, B. O. *J. Chem. Phys.* **1992**, *96*, 1218.

(34) Andersson, K.; Malmqvist, P. A.; Roos, B. O.; Sadlej, A. J.; Wolinski, K. *J. Phys. Chem.* **1990**, *94*, 5483.

(35) Kohn, W.; Becke, A. D.; Parr, R. G. *J. Phys. Chem.* **1996**, *100*, 12974.

(36) Parr, R. G.; Yang, W. *Density Functional Theory of Atoms and Molecules*; Oxford University Press: New York, 1989.

(37) Stratmann, R. E.; Scuseria, G. E.; Frisch, M. J. *J. Chem. Phys.* **1998**, *109*, 8218.

(38) An analysis performed on the $2p_z$ atomic orbital of N^a is provided.

(39) HOMO−17 is the highest-lying of the four MOs that participate in this interaction; there are in- and out-of-phase combinations of the involved fragment orbitals that lie even lower (see Table S1).

(40) Zheng, S.; Phillips, H.; Geva, E.; Dunietz, B. D. *J. Am. Chem. Soc.* **2012**, *134*, 6944.

(41) Tozer, D. J. *J. Chem. Phys.* **2003**, *119*, 12697.

(42) Dreuw, A.; Weisman, J. L.; Head-Gordon, M. *J. Chem. Phys.* **2003**, *119*, 2943.

(43) Dreuw, A.; Head-Gordon, M. *J. Am. Chem. Soc.* **2004**, *126*, 4007.

(44) Yanai, T.; Tew, D. P.; Handy, N. C. *Chem. Phys. Lett.* **2004**, *393*, 51.

(45) This issue was brought to our attention by one of the reviewers, for which we are grateful.

(46) Sinicropi, A.; Pogni, R.; Basosi, R.; Robb, M. A.; Gramlich, G.; Nau, W. M.; Olivucci, M. *Angew. Chem., Int. Ed.* **2001**, *40*, 4185.

(47) Garavelli, M.; Celani, P.; Bernardi, F.; Robb, M. A.; Olivucci, M. *J. Am. Chem. Soc.* **1997**, *119*, 6891.
(48) Reichardt, C.; Guo, C.; Crespo-Hernández, C. E. *J. Phys. Chem. B* **2011**, *115*, 3263.
(49) Richter, M.; Marquetand, P.; González-Vázquez, J.; Sola, I.; González, L. *J. Phys. Chem. Lett.* **2012**, *3*, 3090.
(50) Minns, R. S.; Parker, D. S. N.; Penfold, T. J.; Worth, G. A.; Fielding, H. H. *Phys. Chem. Chem. Phys.* **2010**, *12*, 15607.
(51) Danovich, D.; Shaik, S. *J. Am. Chem. Soc.* **1997**, *119*, 1773.
(52) Duman, S.; Cakmak, Y.; Kolemen, S.; Akkaya, E. U.; Dede, Y. *J. Org. Chem.* **2012**, *77*, 4516.
(53) Dede, Y.; Zhang, X.; Schlangen, M.; Schwarz, H.; Baik, M.-H. *J. Am. Chem. Soc.* **2009**, *131*, 12634.
(54) The NOONs of 1.5 and 0.5 for the S_1 state of **2** show the deviation from a typical HOMO−LUMO excited open-shell singlet state.
(55) Salem, L.; Rowland, C. *Angew. Chem., Int. Ed. Engl.* **1972**, *11*, 92.
(56) Salem, L. *Electrons in Chemical Reactions: First Principles*; John Wiley & Sons: New York, 1982; p 188.
(57) Shaik, S.; Epiotis, N. D. *J. Am. Chem. Soc.* **1978**, *100*, 18.
(58) Shaik, S. S. *J. Am. Chem. Soc.* **1979**, *101*, 3184.
(59) Shaik, S. S.; Epiotis, N. D. *J. Am. Chem. Soc.* **1980**, *102*, 122.
(60) For the role of exchange on two-electron singlet and triplet wave functions, see: Pilar, F. L. *Elementary Quantum Chemistry*, 2nd ed.; McGraw-Hill: New York, 1990; pp 191−214
(61) El-Sayed, M. A. *J. Chem. Phys.* **1963**, *38*, 2834.
(62) El-Sayed, M. A. *Acc. Chem. Res.* **1968**, *1*, 8.
(63) Caldwell, R. A. *Pure Appl. Chem.* **1984**, *56*, 1167.
(64) Zener, C. *Proc. R. Soc. London, Ser. A* **1932**, *137*, 696.
(65) See pp S14−S15 in the Supporting Information.
(66) When the highest ratios of ISC probabilities are considered, the relative rate difference of ISC can reach up to 159. As there is no need to assume similar degrees of rotation for the two species, this assumption is plausible.
(67) Buyuktemiz, M.; Duman, S.; Dede, Y. *J. Phys. Chem. A* **2013**, *117*, 1665.
(68) Grabowski, Z. R.; Rotkiewicz, K.; Rettig, W. *Chem. Rev.* **2003**, *103*, 3899.
(69) Fromherz, P.; Heilemann, A. *J. Phys. Chem.* **1992**, *96*, 6864.
(70) Faulhaber, K.; Granzhan, A.; Ihmels, H.; Viola, G. *Pure Appl. Chem.* **2006**, *78*, 2325.
(71) Ji, S.; Yang, J.; Yang, Q.; Liu, S.; Chen, M.; Zhao, J. *J. Org. Chem.* **2009**, *74*, 4855.
(72) Zhang, X.; Chi, L.; Ji, S.; Wu, Y.; Song, P.; Han, K.; Guo, H.; James, T. D.; Zhao, J. *J. Am. Chem. Soc.* **2009**, *131*, 17452.
(73) Ben-Nun, M.; Martinez, T. J. *Adv. Chem. Phys.* **2002**, *121*, 439.
(74) Vosko, S. H.; Wilk, L.; Nusair, M. *Can. J. Phys.* **1980**, *58*, 1200.
(75) Becke, A. D. *Phys. Rev. A* **1988**, *38*, 3098.
(76) Lee, C. T.; Yang, W. T.; Parr, R. G. *Phys. Rev. B* **1988**, *37*, 785.
(77) Becke, A. D. *J. Chem. Phys.* **1993**, *98*, 5648.
(78) Stephens, P. J.; Devlin, F. J.; Chabalowski, C. F.; Frisch, M. J. *J. Phys. Chem.* **1994**, *98*, 11623.
(79) Hertwig, R. H.; Koch, W. *Chem. Phys. Lett.* **1997**, *268*, 345.
(80) Duman, S. M.S. Thesis, Gazi University, Ankara, Turkey, 2012.
(81) Dunning, T. H. *J. Chem. Phys.* **1989**, *90*, 1007.
(82) Tomasi, J.; Mennucci, B.; Cammi, R. *Chem. Rev.* **2005**, *105*, 2999.
(83) Tomasi, J.; Persico, M. *Chem. Rev.* **1994**, *94*, 2027.
(84) Ruedenberg, K.; Cheung, L. M.; Elbert, S. T. *Int. J. Quantum Chem.* **1979**, *16*, 1069.
(85) Fedorov, D. G.; Gordon, M. S. *J. Chem. Phys.* **2000**, *112*, 5611.
(86) Lefebvre-Brion, H.; Field, R. W. *Perturbations in the Spectra of Diatomic Molecules*; Academic Press: New York, 1986; p 28.
(87) Bethe, H. A.; Salpeter, E. E. *Quantum Mechanics of One- and Two-Electron Atoms*; Springer: Berlin, 1957; p 170.
(88) Forst, W. *Unimolecular Reactions: A Concise Introduction*; Cambridge University Press: Cambridge, U.K., 2003.
(89) Aquilante, F.; De Vico, L.; Ferré, N.; Ghigo, G.; Malmqvist, P.-å.; Neogrády, P.; Pedersen, T. B.; Pitoňák, M.; Reiher, M.; Roos, B. O.; Serrano-Andrés, L.; Urban, M.; Veryazov, V.; Lindh, R. *J. Comput. Chem.* **2010**, *31*, 224.
(90) Karlström, G.; Lindh, R.; Malmqvist, P.-Å.; Roos, B. O.; Ryde, U.; Veryazov, V.; Widmark, P.-O.; Cossi, M.; Schimmelpfennig, B.; Neograd y, P.; Seijo, L. *Comput. Mater. Sci.* **2003**, *28*, 222.
(91) Schmidt, M. W.; Baldridge, K. K.; Boatz, J. A.; Elbert, S. T.; Gordon, M. S.; Jensen, J. H.; Koseki, S.; Matsunaga, N.; Nguyen, K. A.; Su, S.; Windus, T. L.; Dupuis, M.; Montgomery, J. A., Jr. *J. Comput. Chem.* **1993**, *14*, 1347.
(92) Frisch, M. J.; Trucks, G. W.; Schlegel, H. B.; Scuseria, G. E.; Robb, M. A.; Cheeseman, J. R.; Montgomery, J. A., Jr.; Vreven, T.; Kudin, K. N.; Burant, J. C.; Millam, J. M.; Iyengar, S. S.; Tomasi, J.; Barone, V.; Mennucci, B.; Cossi, M.; Scalmani, G.; Rega, N.; Petersson, G. A.; Nakatsuji, H.; Hada, M.; Ehara, M.; Toyota, K.; Fukuda, R.; Hasegawa, J.; Ishida, M.; Nakajima, T.; Honda, Y.; Kitao, O.; Nakai, H.; Klene, M.; Li, X.; Knox, J. E.; Hratchian, H. P.; Cross, J. B.; Bakken, V.; Adamo, C.; Jaramillo, J.; Gomperts, R.; Stratmann, R. E.; Yazyev, O.; Austin, A. J.; Cammi, R.; Pomelli, C.; Ochterski, J. W.; Ayala, P. Y.; Morokuma, K.; Voth, G. A.; Salvador, P.; Dannenberg, J. J.; Zakrzewski, V. G.; Dapprich, S.; Daniels, A. D.; Strain, M. C.; Farkas, O.; Malick, D. K.; Rabuck, A. D.; Raghavachari, K.; Foresman, J. B.; Ortiz, J. V.; Cui, Q.; Baboul, A. G.; Clifford, S.; Cioslowski, J.; Stefanov, B. B.; Liu, G.; Liashenko, A.; Piskorz, P.; Komaromi, I.; Martin, R. L.; Fox, D. J.; Keith, T.; Al-Laham, M. A.; Peng, C. Y.; Nanayakkara, A.; Challacombe, M.; Gill, P. M. W.; Johnson, B.; Chen, W.; Wong, M. W.; Gonzalez, C.; Pople, J. A. *Gaussian 03*, revision C.02; Gaussian, Inc.: Wallingford, CT, 2004.